Baffled-Tube Ram Accelerator Operation with Aluminum Projectiles

John Correy[1], Jackson Clevenger[1], Carl Knowlen[1], Andrew Higgins[2]
[1]William E. Boeing Department of Aeronautics and Astronautics, University of Washington
Seattle, WA 98195, USA
[2]Department of Mechanical Engineering, McGill University
Montreal, Quebec, Canada

1 Introduction

The ram accelerator is a chemical mass driver using in-tube ramjet propulsive cycles to generate thrust [1]. In the smooth bore ram accelerator (SBRA), supersonic projectiles accelerate through premixed propellant at velocities less than Chapman-Jouguet (CJ) detonation speed with subsonic combustion occurring behind projectile, as shown in Fig. 1. Propellant heat release thermally chokes the flow and stabilizes a shock wave on projectile aft-body, which results in a region of high pressure that generates thrust. The theoretical operating velocity range of the thermally choked ram accelerator (TCRA) propulsive mode is 0.5 km/s to 3.5 km/s. Because of its hypersonic velocity potential, scalability, and tailorable acceleration, the ram accelerator is envisioned to replace initial rocket stages of orbital space launchers [2] and has been proposed for use in industrial applications such as hard rock mining and tunneling [3].

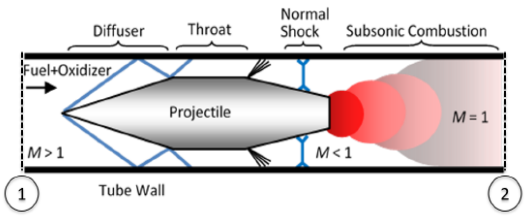

Figure 1: Flow field of TCRA propulsive mode in smooth-bore tube and control volume boundaries for 1-D analysis.

Ram accelerator operation in the TCRA propulsive mode has been demonstrated with muzzle velocities up to 2.6 km/s and at in-tube Mach numbers ranging from approximately 2.5 to 5. Empirically it was found that the maximum reliable propellant heat release for TCRA operation in a SBRA was limited to about one third that available in methane-oxygen propellant [4, 5]. When the heat release was too high, the shock wave system on the projectile aft-body was pushed too far forward, causing a combustion-driven wave unstart. The resulting shock wave ahead of the projectile, which may become an overdriven detonation wave, shifts the highest pressure to the nosecone and thereby produces high deceleration.

The baffled tube ram accelerator (BTRA) was proposed as a means to prevent wave unstarts and enable operation in propellants with very high heat release [5]. The BTRA consists of a tube with washer-like baffles that allow unreacted propellant to be ram compressed in the chambers around its shoulder and prevent combustion from pushing the leading edge of high pressure region ahead of projectile, as shown in Fig. 2. By preventing combustion-driven unstarts, the BTRA allows for operation with propellants having much higher heat release and more potential thrust at a given fill pressure than possible with the TCRA propulsive mode in the SBRA. The efficacy of the BTRA concept has been established in a 38-mm-bore apparatus over a velocity range of 0.65 km/s to 1.4 km/s, Mach number range of 2 to 4.5, and at fill pressures up to 4.2 MPa with propellants having up to twice the heat release of those used in the SBRA [6, 7]. Recent experimental results with aluminum projectiles are presented here.

Correspondence to: knowlen@aa.washington.edu

2 Theory

Modeling of TCRA thrust performance in a SBRA is readily accomplished by applying one-dimensional conservation equations between stations 1 and 2 in Fig. 1 [1, 8]. To account for the volume occupied by internal rails and baffles inside a BTRA, the baffle chamber volume is equated to an equivalent smooth bore tube having same amount of propellant per unit tube length, as shown in Fig. 3. The rail volume, V_r, is subtracted from sum of the volumes of cylindrical chamber, $V_c = \pi d_c^2 L_c$, and baffle port, $V_b = \pi d_b^2 L_b$. The baffle volume factor, β, defined as the effective tube-to-baffle bore area ratio, A_{eff}/A_b, is determined from the net volume of baffle chamber normalized by cylindrical volume of the baffle port extended for the chamber length as follows:

$$\beta = \frac{A_{eff}}{A_b} = \frac{V_c + V_b - V_r}{V_b\left(1 + L_c/L_b\right)} = \frac{d_{eff}^2}{d_b^2} \tag{1}$$

One-dimensional conservation equations applied to the control volume of the effective tube element shown in Fig. 3 can determine the net TCRA thrust, F_{TCRA}, for a given in-tube Mach number and propellant. Thrust normalized to fill pressure, P_1, and effective tube area, A_{eff}, defines the non-dimensional thrust, I_{TCRA}, as shown in Eq. 2. Forward acting forces are applied to both the baffles and projectile during BTRA operation. Assuming the net TCRA thrust was distributed on an area basis between the baffle, F_b, and projectile, F_p, results in Eq. 3.

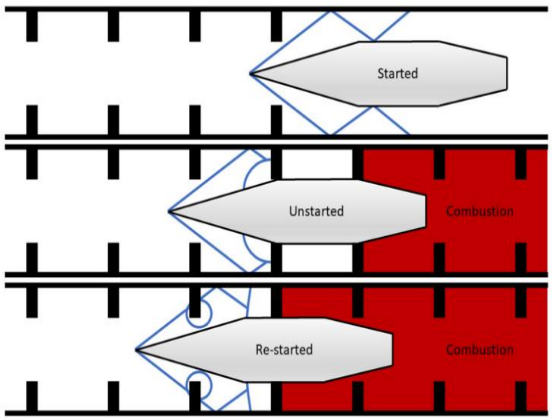

Figure 2: Projectile unstarts upon entering baffle port and restarts when shoulder overtakes radial expanding shock wave.

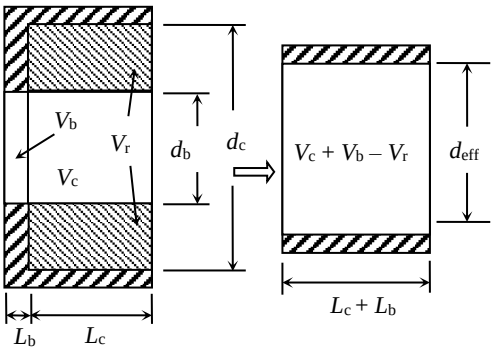

Figure 3: Effective diameter geometry for BTRA chamber.

$$I_{\mathrm{TCRA}} = \frac{F_{\mathrm{TCRA}}}{P_1 A_{\mathrm{eff}}} = M_1 \frac{\gamma_1}{\gamma_2}(1+\gamma_2)\sqrt{\left(\frac{\gamma_2-1}{\gamma_1-1}\right)\frac{\frac{h_1}{c_{p1}T_1}+\frac{M_1^2(\gamma_1-1)}{2}+Q}{\frac{h_2}{c_{p2}T_2}+\frac{(\gamma_2-1)}{2}}} - (1+\gamma_1 M_1^2) \tag{2}$$

$$I_{\mathrm{TCRA}} = \frac{F_{\mathrm{p}}+F_{\mathrm{b}}}{P_1 A_{\mathrm{eff}}} = \frac{I_{\mathrm{TCRA}}\times A_{\mathrm{b}}}{A_{\mathrm{eff}}} + \frac{I_{\mathrm{TCRA}}\times(A_{\mathrm{eff}}-A_b)}{A_{\mathrm{eff}}} = \frac{I_{TCRA}}{\beta} + \frac{I_{TCRA}(\beta-1)}{\beta} = I_{\mathrm{p}} + I_{\mathrm{b}} \tag{3}$$

Thus, the non-dimensional projectile thrust, when normalized to the baffle port area, can then be shown to be equal to the non-dimensional TCRA thrust for the effective tube segment in Fig. 3 as follows:

$$I_{\mathrm{TCRA}} = I_{\mathrm{p}} \times \beta = \frac{F_{\mathrm{p}}}{P_1 A_{\mathrm{eff}}}\frac{A_{\mathrm{eff}}}{A_{\mathrm{b}}} = \frac{F_{\mathrm{p}}}{P_1 A_{\mathrm{b}}} \tag{4}$$

This results in projectile thrust being dependent on β as shown in Fig. 4. The SBRA non-dimensional thrust profile for a workhorse propellant ($\beta = 1.0$) was also plotted along with those predicted for the BTRA propellant used in experiments with baffled-tube configurations having average baffle volume ratios of $\beta = 2.123$, 2.168, and 2.825. It is apparent that the SBRA generates higher thrust at Mach numbers less than 3.5. Conversely, BTRA has a wider operational Mach number range and its thrust increases when the baffle chamber diameter decreases to reduce β. Note, predicted peak thrust is increased by ~18% with respect to that of the $\beta = 2.123$ configuration by reducing chamber diameter to get $\beta = 1.8$ (Fig. 4). Testing this new baffle insert design is planned for future work.

3 Experimental Test Facility

The ram accelerator facility and supporting subsystems have been described in detail elsewhere [6], thus only the baffle designs, BTRA test section, and projectiles were presented here. Baffle insert designs in Fig. 5 had the same baffle and rail dimensions (listed in caption), however, their chamber parameters varied. The open chamber design in Fig. 5a provided maximum volume for propellant and highest baffle volume ratio of $\beta = 2.825$. The cylindrical shell extruded from baffle periphery reduced chamber diameter by ~17% for the baffle insert designs in Figs. 5b and 5c. The baffle insert in Fig. 5b ($\beta = 2.179$) had slotted chamber ports to mitigate interference with electromagnetic sensors that protruded into the chamber whenever inserts inadvertently shifted in experiments. The baffle inserts with circular chamber ports (Fig. 5c) had the lowest baffle volume ratio ($\beta = 2.117$) and thus highest thrust potential. They were placed throughout the last two BTRA tubes except at the instrument ports.

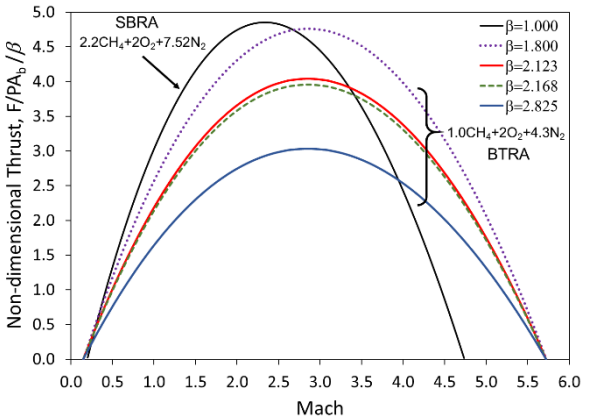

Figure 4: Non-dimensional thrust for baffle volume ratios, β, used in BTRA experiments.

The BTRA test section was comprised of four two-meter-long shell tubes with various combinations of baffle inserts as shown in Fig. 6. Baffle inserts with largest β values (blue) were place in the first tube to enable initiation of BTRA operation at the lowest feasible Mach number. Slotted baffles (yellow) then followed and were also placed at the instrument ports between the circular-port baffles (red). The average baffle volume factor values for each BTRA tube (top to bottom, $\beta = 2.825$, 2.168, 2.123, 2.123) were used in determining theoretical non-dimensional projectile thrust (Eq. 4) for comparison with experiment. Average thrust was determined from entrance and exit velocity data for each BTRA tube.

(a) (b) (c)

Figure 5: Baffle insert designs with overall length of 35.7 mm that includes the 6.35-mm-thick baffle with 38.2-mm-port and 76.2-mm-outer diameter. (a) Open chamber, $\beta = 2.825$, (b) Slotted chamber ports, $\beta = 2.179$, (c) Circular chamber ports, $\beta = 2.117$.

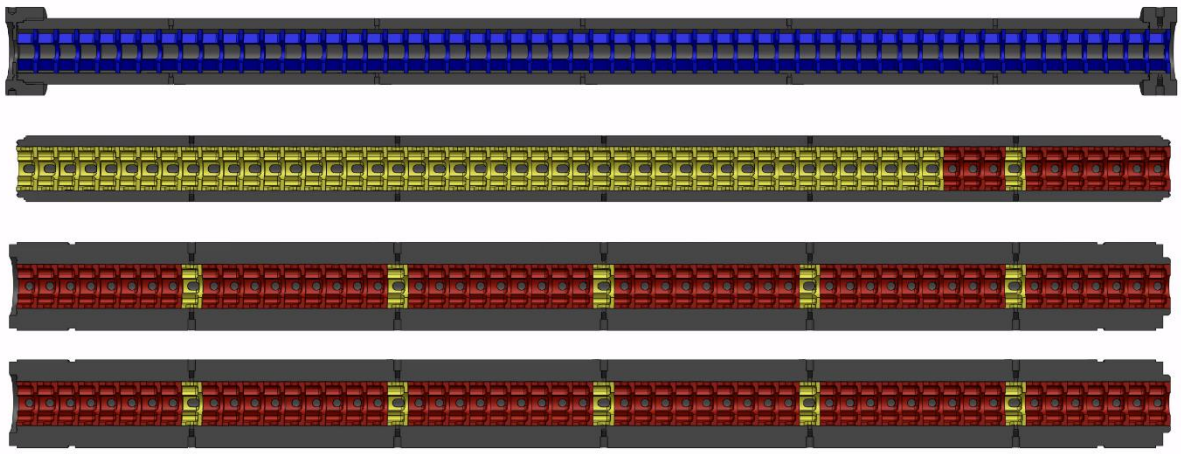

Figure 6: Two-meter-long shell tubes with 56 baffle inserts in each. Projectiles enter left to right.

The axisymmetric projectiles were comprised of nosecone, cylindrical shoulder section, and tail frustum pieces that threaded together as shown in Fig. 7. These projectiles had 15º nosecones, 12º tail frusta, and were fabricated from aluminum alloy (6061-T6). Their shoulder diameters were 35.1 mm and shoulder lengths were 71.4 mm. The projectile masses (m_p) were either 158 g or 206 g, depending on wall thickness. A neodymium magnet in the projectile nosecone enabled its tracking via electromagnetic sensors to determine time-of-passage, velocity, and acceleration throughout the test section.

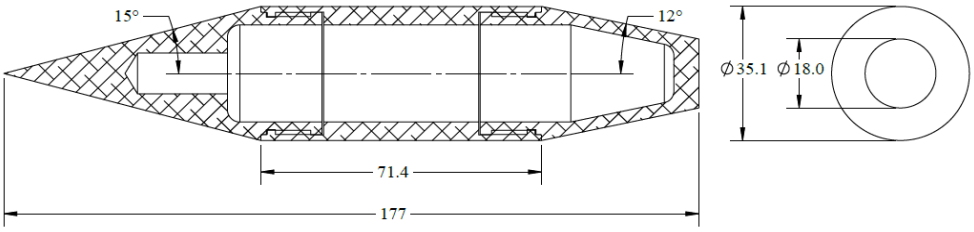

Figure 7: Three-piece Al alloy projectile design (mm); thin-wall m_p = 158 g, thick-wall m_p = 206 g.

4 Experimental Procedures and Results

All but two experiments presented here were carried out with a nominal propellant of $1.0CH_4+2O_2+4.3N_2$ at fill pressures ranging from 2.17 MPa to 4.24 MPa. Entrance velocities were 0.84 km/s ±0.02 km/s unless noted otherwise, which corresponded to in-tube entrance Mach numbers of ~2.4. Plotted in Fig. 8 were the velocity-distance data from three sets of experiments and their corresponding non-dimensional thrusts compared with theory. For each experiment, the shot reference number, fill pressure(s), and projectile mass were included in the legends.

The thin-walled aluminum projectile velocity-distance data plotted in Fig. 8a included one test firing with a solid polycarbonate projectile that had the same external geometry except for its longer shoulder (107.1-mm) [9]. At a fill pressure of 2.17 MPa, the aluminum projectile steadily accelerated up to 1.42 km at the BTRA exit. At the same fill pressure, the polycarbonate projectile accelerated up to a speed of ~1.3 km/s before its thrust abruptly decreased in the last meter of the test section. This implied that the projectile may have been damaged due to aerothermal heating, which resulted in increased drag due to nosecone deformation and/or reduction in thrust due to tail frustum deterioration [9]. When the aluminum projectile entered the propellant with 23% higher fill pressure (2.67 MPa), it was accelerated up to an exit velocity of 1.51 km/s (Mach ~4.3). The corresponding thrust averaged over the 8-m-length of the BTRA test section increased by ~21%, which indicates that thrust scaled linearly with pressure as expected. Note the projectile continued to accelerate in the evacuated smooth bore tubes after the BTRA test section due to the expansion of the high pressure combustion products, gaining another ~0.1 km/s from the “drift tube” boost. These thin-walled projectiles were not fired into propellant with higher fill pressure because prior testing had shown that they were subject to structural failure above ~3 MPa.

Pressure sweep data for thick-walled aluminum projectiles were plotted in Figs. 8b. Due to tube wall thickness differences, the fill pressure was limited to 3.20 MPa in the first two BTRA shell tubes (1st stage) and was increased up to 4.24 MPa in the last two BTRA tubes (2nd stage). The first firing had both stages filled to 3.20 MPa with the nominal propellant composition. In this case the projectile accelerated up to 1.41 km/s by the end of the test section. Increasing fill pressure in the 2nd stage by ~16% to 3.72 MPa increased exit velocity to 1.47 km/s. The corresponding thrust averaged over the 4-m-long 2nd stage increased by ~26%, which was more than expected from pressure scaling. The thrust was again increased in the 2nd stage by raising the pressure 4.24 MPa, however, near the end of this stage the projectile unstarted, i.e., the combustion-driven shock wave on the tail frustum was thrust ahead of the projectile throat, resulting in abrupt deceleration [4].

Two potential causes for this unstart were projectile degradation in high pressure propellant and/or too much increase in propellant heat release due to increased fill pressure (resulting from decreased product dissociation). To determine which cause was likely responsible for the unstart, two additional experiments were carried out at the same fill pressures with a slightly fuel-enriched propellant ($1.2CH_4+2O_2+4.3N_2$) to reduce heat release and the potential for aluminum burning. Velocity-distance data from these tests along with data from the one that unstarted were plotted in Fig. 8c. In the first of these firings, the entrance velocity was ~0.03 km/s lower than expected and the projectile accelerated throughout the test section up to an exit velocity of 1.44 km/s. This exit velocity, however, was less than the peak velocity attained by the projectile before it unstarted in the prior firing (~1.47 km/s). Thus a second shot in fuel-rich propellant was conducted with entrance velocity increased to 0.94 km/s. In this case, the projectile accelerated throughout the test section up to an exit velocity of 1.51 km/s (Mach ~4.3). This result indicated that pressure influences on heat release were mitigated by addition of fuel and that operation at same Mach number as seen at lower fill pressure was possible with more massive projectiles. (Note, the drift tube boost was not experienced in this firing because the downstream tubes were filled with inert gas (He) to strip the combustion products from the projectile.)

Experimental average non-dimensional thrust data in each 2-m-long BTRA tube for aluminum projectiles were plotted in Fig. 8d along with theory that was adjusted for the corresponding baffle volume factors. Only data from experiments using $1.0CH_4+2O_2+4.3N_2$ propellant were plotted. The experimental thrust in all cases was less than theory predicted, with the greatest discrepancies (~50%)

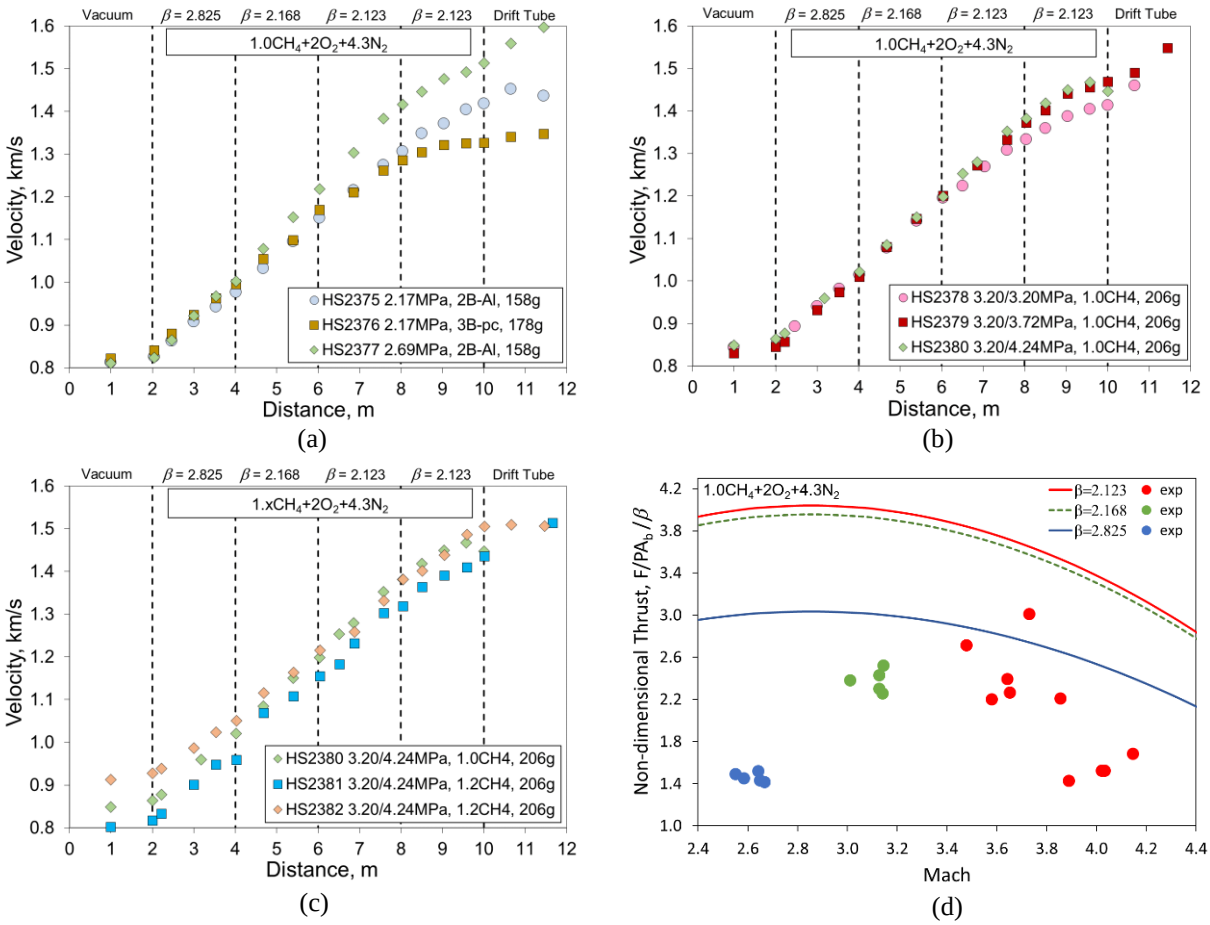

Figure 8: Experimental BTRA velocity data: (a) Thin-walled 2B-Al and solid 3B-PC projectiles, (b) Thick-walled 2B-Al pressure sweep, (c) Thick-walled 2B-Al in less energetic propellant, (d) Experimental BTRA non-dimensional thrust data with theory for various baffle volume ratios, β.

in the first BTRA tube ($\beta = 2.825$) and at lowest average Mach number (~2.6). These results may be skewed toward the low side due to starting transients even though this process was very repeatable. In the second BTRA tube ($\beta = 2.168$), the thrust at Mach ~3.1 was ~32% less than predicted. In the last two BTRA tubes ($\beta = 2.123$), the thrust was ~30% lower at Mach ~3.6 and ~48% lower at Mach ~4.0. Experimental BTRA thrust characteristics have been shown to be dependent on baffle insert and projectile geometries [6, 9]. Thus there is the possibility of substantially increasing it with optimal baffle and projectile designs. Linearly extrapolating the thrust in the last two BTRA tubes indicates that the drag will equal thrust at a peak Mach number of ~4.6 in this propellant, which is substantially lower than predicted by theory. Nonetheless, higher velocities will be attainable by making a transition to propellants with higher sound speeds to reduce operational Mach number. In this manner, velocities greater than 2.5 km/s appear to be feasible with the BTRA configurations used here.

5 Conclusions

Aluminum projectiles were accelerated in an 8-m-long BTRA test section up to velocities of 1.51 km/s at in-tube Mach numbers of ~4.3 in $1.0CH_4+2O_2+4.3N_2$ propellant at 2.69 MPa fill pressure. At 4.24 MPa, the propellant needed to be fuel-enriched to 1.2CH4 to enable operation up to the same velocity. A revision to the theory for thermally choked ram accelerator propulsive cycle in the BTRA was proposed that assumed thrust was distributed between the projectile and baffle wall on an area proportional basis. This resulted in thrust predictions that were 40% to 100% higher than experiment. Nonetheless, robust and repeatable projectile accelerations were demonstrated that indicated operation at velocities greater than 1.6 km/s (Mach ~4.6) may be possible in CH_4-O_2-N_2 propellants.

Acknowledgement

Thanks for experiment assistance from K. Laslett-Vigil, A. Fenchenko, B. Anderson, B. Ament, C. Park, G. Rathnayake, G. Gallagher, N. Pravind, and V. Hernadez. This research was funded by General Hypersonics, Inc., which has licensed the described technology from the University of Washington.

References

[1] Bruckner AP, Knowlen C, Hertzberg A, Bogdanoff DW. (1991) Operational Characteristics of the Thermally Choked Ram Accelerator. J Prop & Power. 7:828.

[2] Knowlen C, Joseph B, and Bruckner AP. (2007) Ram Accelerator as an Impulsive Space Launcher: Assessment of Technical Risks. International Space Development Conference, Dallas, TX.

[3] Russell M, Urselmann R, Bernhard D, Colburn B, Russell C, Durkee KJ. (2021) Robotic Mining and Micro Tunneling Using Hypersonic Projectile Impact Technology. RET Conference. Las Vegas, NV.

[4] Higgins AJ, Knowlen C, and Bruckner AP. (1998) Ram Accelerator Operating Limits, Part 2: Nature of Observed Limits. J Prop & Power. 14:959.

[5] Knowlen C, Glusman J, Bruckner AP, Higgins AJ. (2016) Experimental Investigation of a Baffled-Tube Ram Accelerator. AIAA 2016-4813.

[6] Correy J, Leege BJ, Bernhard D, Ginos J, Yancey C, Knowlen C, Higgins AJ. (2023) Investigation of Baffled-Tube Ram Accelerator Configurations. AIAA 2023-2186.

[7] Correy J, Bernhard D, Ginos J, Knowlen C, Higgins AJ. (2024) Mach Number Effects on Baffled-Tube Ram Accelerators. AIAA 2024-1610.

[8] Sasoh A, Hamate Y, Takayama K. (2001) Small-Bore Ram Accelerator Operation. J Prop & Power. 17:622.

[9] Correy J, Ginos J, Alam JAR, Knowlen C, Higgins AJ. (2025) Projectile Geometry Effects on Baffled-Tube Ram Accelerator Thrust. AIAA 2025-1725.